

Shell model study of ^{40}Ca muon capture and the $(0^+, 0) \rightarrow (0^-, 2626)$ axial charge transition

T.P. Gorringe

Department of Physics and Astronomy, University of Kentucky, Lexington, KY 40506

(February 9, 2020)

Abstract

We report results from shell model studies of muon capture on ^{40}Ca to low-lying levels of ^{40}K . We discuss the comparison between calculated capture rates, measured capture rates and analogous transitions in (e, e') scattering in terms of the particle-hole structure of the ^{40}Ca - ^{40}K nuclei. We highlight the $^{40}\text{Ca}(0^+, 0) \rightarrow ^{40}\text{K}(0^-, 2626)$ axial charge transition and its sensitivity to the induced pseudoscalar coupling g_p of the proton's weak interaction. In addition, we address the hindrance of unique first-forbidden transitions due to particle-hole interactions and the emergence of allowed Gamow-Teller transitions due to ground state correlations. Lastly, we examine the longitudinal alignment of ^{40}K recoils following muon capture, and discuss this possibility for independently determining the induced coupling g_p .

23.40.-s, 23.40.Hc, 27.40.+z

I. INTRODUCTION

Studies of muon capture on complex nuclei have spanned nearly fifty years. The early work [1–3] was devoted to establishing the universal V-A character of nuclear muon capture, while later work has focused on induced currents [4], second-class currents [5,6] and non V - A interactions [7]. Muon capture is also a valuable window on particle-hole excitations and spin-isospin modes in nuclei [8], it complementing the information that is obtained from beta-decay, electron scattering and charge exchange reactions.

Of particular interest in nuclear muon capture is the induced pseudoscalar coupling g_p of the proton’s weak interaction. For the free proton, the coupling g_p is predicted to few-percent accuracy by symmetry arguments and thereby represents an important test of low energy QCD [9–11]. For the bound proton, its medium modification is sensitive to effects that range from pion exchange currents and Δ -hole excitations to partial restoration of chiral symmetry [12–14]. Indeed, some suggestions of a large A -dependent renormalization of the induced coupling g_p have been published in the literature [12,15].

Measday and Stocki [16] have recently published new experimental results on γ -ray spectra from muon capture on ^{40}Ca that include determinations of partial rates and rate limits for numerous $^{40}\text{Ca}(\mu,\nu)^{40}\text{K}$ transitions. Their data are noteworthy as the heaviest nucleus on which (μ,ν) reactions have been clearly identified. Their data show evidence of excitations that range from allowed Gamow-Teller transitions to highly ℓ -forbidden transitions.

Most important is their observation of the $^{40}\text{Ca}(0^+, 0) \rightarrow ^{40}\text{K}(0^-, 2626)$ axial charge transition. In nuclear beta decay such $0^+ \leftrightarrow 0^-$ transitions have been extensively studied – both experimentally and theoretically – and nowadays represent our clearest evidence for exchange currents in complex nuclei. In muon capture the only known example of a $0^+ \leftrightarrow 0^-$ first forbidden transitions was the celebrated $^{16}\text{O}(0^+, 0) \rightarrow ^{16}\text{N}(0^-, 120)$ transition, it having been studied by many authors in the context of the coupling g_p . In light of suggestions of an A -dependent renormalization of the induced coupling g_p , the $^{40}\text{Ca}(0^+, 0) \rightarrow ^{40}\text{K}(0^-, 2626)$ transition represents a valuable data point for experimentally accessing g_p in medium-weight

nuclei.

Also interesting are two unique first forbidden transitions and one allowed Gamow Teller transition: ${}^{40}\text{Ca}(0^+, 0) \rightarrow {}^{40}\text{K}(2^-, 800)$, ${}^{40}\text{Ca}(0^+, 0) \rightarrow {}^{40}\text{K}(2^-, 2047)$ and ${}^{40}\text{Ca}(0^+, 0) \rightarrow {}^{40}\text{K}(1^+, 2290)$. One motivation for investigating unique first-forbidden transitions stems from the large quenching of such transitions in nuclear β -decay, such quenching arising from the coherent effects of the repulsive $T=1$ particle-hole interaction. One motivation for investigating allowed Gamow-Teller transitions stems from their absence in a simple closed-shell description of doubly-magic ${}^{40}\text{Ca}$, their emergence arising from the multi-particle, multi-hole admixtures in the ${}^{40}\text{Ca}$ ground state. In addition, the ${}^{40}\text{Ca}(0^+, 0) \rightarrow {}^{40}\text{K}(2^-, 800)$ and ${}^{40}\text{Ca}(0^+, 0) \rightarrow {}^{40}\text{K}(2^-, 2290)$ transitions have well known analogs in (e, e') inelastic scattering [17–19] and charge exchange reactions [20,21]. The comparison between (μ^-, ν) capture rates and analogous (e, e') transitions thus provides a valuable cross-check for the ${}^{40}\text{Ca}(\mu, \nu){}^{40}\text{K}$ data and a valuable comparison for the ${}^{40}\text{Ca}(\mu, \nu){}^{40}\text{K}$ calculations.

The ${}^{40}\text{Ca}(\mu, \nu){}^{40}\text{K}$ data are also interesting in the broader context of the shell structure of the $A \sim 40$ region. Warburton and co-workers have published a series of articles [22–26] on mass $34 \leq A \leq 50$ nuclei that include comprehensive studies of $\Delta J^\pi = 0^-$ β decays and their enhancement due to exchange currents effects, $\Delta J^\pi = 2^-$ β decays and their hindrance due to core polarization effects, and the evolving nuclear structure of the $A \sim 40$ mass region. Weak transition rates on doubly magic ${}^{40}\text{Ca}$ are the archetypal benchmark for such model calculations.

Herein we report results from shell model studies of muon capture on ${}^{40}\text{Ca}$. In Secs. II and III respectively we describe the details of the shell model calculations and the capture rate calculations. In Sec. IV we compare the calculated (μ, ν) transition rates with the recent data of Measday and Stocki [16] and the earlier data of Igo-Kemenes *et al.* [27] in the context of the particle-hole structure of the ${}^{40}\text{Ca}-{}^{40}\text{K}$ nuclear wavefunctions. In particular, we discuss the emergence of the $(0^+, 0) \rightarrow (1^+, 2290)$ allowed Gamow-Teller transition, the hindrance of the $0^+ \rightarrow 2^-$ unique first-forbidden transitions, and the sensitivity to the induced pseudoscalar coupling g_p of the ${}^{40}\text{Ca}(0^+, 0) \rightarrow {}^{40}\text{K}(0^-, 2626)$ axial charge transition. Finally, in Sec. V we

briefly consider the longitudinal alignment of ${}^{40}\text{K}$ recoils following ${}^{40}\text{Ca}$ capture, and the dependence of the alignment on the coupling g_p .

II. SHELL MODEL CALCULATIONS

The simplest description of muon capture from the ${}^{40}\text{Ca}$ ground state to the low-lying ${}^{40}\text{K}$ states involves a fully filled sd-shell initial state and various $(\text{sd})^{-1}(\text{pf})^1$ particle-hole final states. This model infers a significant number of forbidden transitions but no allowed transitions as all spin-orbit partners in the ${}^{40}\text{Ca}$ ground state are fully filled. It implies that data for allowed transitions will have interesting sensitivity to the multi-particle, multi-hole admixtures in the ${}^{40}\text{Ca}$ g.s. wavefunction and data for forbidden transitions will have interesting sensitivity to the particle-hole interaction in the $A \sim 40$ mass region.

The ${}^{40}\text{K}$ level diagram of Fig. 1 reveals one negative parity quadruplet with spin-parities $J^\pi = 4^-, 3^-, 2^-$ and 5^- and excitation energies 0, 30, 800 and 891 keV and another negative parity quadruplet with spin-parities $J^\pi = 2^-, 3^-, 1^-$ and 0^- and excitation energies 2047, 2070, 2104 and 2626 keV. The quadruplets are consistent with low-lying negative parity ${}^{40}\text{K}$ states involving $(d_{3/2})^{-1}(f_{7/2})^1$ particle-hole configurations, which yield the $J^\pi = 2^-$ - 5^- quadruplet, and $(d_{3/2})^{-1}(p_{3/2})^1$ particle-hole configurations, which yield the $J^\pi = 0^-$ - 3^- quadruplet. In addition, the four lowest-lying positive parity states, with spin-parities $J^\pi = 0^+, 2^+, 3^+$ and 1^+ and excitation energies 1632, 1959, 2260 and 2290 keV, were identified by Davis *et al.* [28] as consistent with expectations of low-lying $(d_{3/2})^{-2}(f_{7/2})^2$ excitations with the two $f_{7/2}$ -particles coupled to $J = 0$ and the two $d_{3/2}$ -holes coupled to $J = 0$ -3. At higher excitation energies the increasing level density makes meaningful assignments between model configurations and experimental levels much more difficult.

Below we describe the model spaces and residual interactions we have employed in our calculations of the muon capture rates and the ${}^{40}\text{K}$ recoil alignments. Our basic philosophy was to utilize well-known, well-tested models “off-the-shelf”, *i.e.* not fine tuning any model parameters. Our model calculations were performed utilizing the OXBASH code [29].

A. $A = 40$ model spaces and residual interactions

Our primary calculations of ${}^{40}\text{Ca}(\mu, \nu){}^{40}\text{K}$ capture were conducted using the sd-pf model space and the WBMB interaction [30]. The WBMB interaction comprises the sd interaction of Wildenthal [31], the pf interaction of McGory [32], and a modified Millener-Kurath interaction for the cross-shell matrix elements [33]. As discussed in Ref. [22], the sd-pf shell energy gap was empirically adjusted to reproduce the $A = 35\text{-}41$ binding energies and the $d_{3/2}f_{7/2} \leftrightarrow d_{3/2}f_{7/2}$, $d_{3/2}p_{3/2} \leftrightarrow d_{3/2}p_{3/2}$ two-body matrix elements were empirically adjusted to reproduce the low-lying $A = 40$ particle-hole states.

Two versions of WBMB calculations were carried out. In both versions of the WBMB model the negative-parity ${}^{40}\text{K}$ states comprised one particle in the fp shell and one hole in the sd shell, *i.e.* $(sd)^{23}(pf)^1$ configurations, and the positive-parity ${}^{40}\text{K}$ states comprised two particles in the fp shell and two holes in the sd shell, *i.e.* $(sd)^{22}(pf)^2$ configurations. However, to enable the investigation of ground state correlations we employed ${}^{40}\text{Ca}$ wavefunctions with both a pure $(sd)^{24}$ configuration, our so-called $0 \hbar\omega$ WBMB calculation, and a mixed $(sd)^{24} + (sd)^{22}(pf)^2$ configuration, our so-called $(0+2) \hbar\omega$ WBMB calculation. We caution the reader the WBMB interaction was originally developed and generally applied in pure $N \hbar\omega$ model spaces, although the effects of $(0+2) \hbar\omega$ mixing on hypothetical ${}^{40}\text{K} \rightarrow {}^{40}\text{Ca}$ beta-decays was discussed in Ref. [23].¹

We also performed calculations that employed a smaller $d_{3/2}\text{-}f_{7/2}$ model space but allowed a richer $0\text{-}8 \hbar\omega$ particle-hole spectrum. These calculations used the single particle energies and two-body matrix elements of Sakakura, Arima and Sebe [34] which is hereafter denoted as the SAS interaction. This interaction was used in Ref. [34] to study the effects of multi-particle, multi-hole admixtures in 0^+ levels of ${}^{40}\text{Ca}$. While the smaller $d_{3/2}\text{-}f_{7/2}$ space is obviously unable to fully describe all low-lying ${}^{40}\text{K}$ particle-hole levels – it missing the $f_{7/2}^{-1}$ –

¹The correct treatment of $(0+2)\hbar\omega$ mixing is a well-known difficulty in shell model calculations. See Ref. [22] for a discussion of $(0+2)\hbar\omega$ mixing in the $A \sim 40$ mass region.

$p_{3/2}^1$ states – it renders some insight into the multi-particle, multi-hole components in the ^{40}Ca ground state wavefunction and their influence on the (μ, ν) transitions.

B. ^{40}K excitation energies and wavefunction configurations

The WBMB calculations exactly reproduces the excitation energies of the ^{40}K lower-lying $J^\pi = 4^-, 3^-, 2^-, 5^-$ quadruplet and the ^{40}K higher-lying $J^\pi = 2^-, 3^-, 1^-, 0^-$ quadruplet due to the aforementioned adjustments of the $d_{3/2}f_{7/2} \leftrightarrow d_{3/2}f_{7/2}$, $d_{3/2}p_{3/2} \leftrightarrow d_{3/2}p_{3/2}$ two-body matrix elements. Within the WBMB model the $J^\pi = 4^-, 3^-, 2^-, 5^-$ quadruplet has $d_{3/2}^{-1}f_{7/2}^1$ occupancies that range from 92 to 98% and the $J^\pi = 2^-, 3^-, 1^-, 0^-$ quadruplet has $d_{3/2}^{-1}p_{3/2}^1$ occupancies that range from 75 to 99% (the occupancies are consistent with the compilation of spectroscopic factors in Endt *et al.* [35]). By comparison the WBMB model yields low-lying ^{40}K positive parity states that are typically 1 MeV under-bound and have somewhat exaggerated energy spacings – although the model does reproduce the $J^\pi = 0^+, 2^+, 3^+, 1^+$ level ordering. While the $J^\pi = 0^+, 2^+, 3^+$ states have dominant $d_{3/2}^{-2}f_{7/2}^2$ character the $J^\pi = 1^+$ state is a more fragmented mixture of the permissible 2p-2h configurations.

The SAS model reproduces the excitation energies of the lower-lying negative-parity ^{40}K quadruplet with spin-parities $J^\pi = 4^-, 3^-, 2^-, 5^-$ to accuracies of roughly 200 keV. The corresponding SAS wavefunctions have their largest contributions from $d_{3/2}^{-1}f_{7/2}^1$ configurations (43-55%) but with substantial contributions from $d_{3/2}^{-3}f_{7/2}^3$ configurations (31-40%). The $J^\pi = 0^+, 2^+, 3^+, 1^+$ level ordering is reproduced by the SAS model although the $J^\pi = 0^+, 2^+$ states are over-bound by roughly 1 MeV. All four positive parity states have their largest contributions from $d_{3/2}^{-2}f_{7/2}^2$ configurations (42-61%) but with substantial contributions from $d_{3/2}^{-4}f_{7/2}^4$ configurations (34-40%). Of course the SAS model and $d_{3/2}-f_{7/2}$ space is unable to account for the higher-lying negative-parity ^{40}K quadruplet with its dominant $d_{3/2}^{-1}p_{3/2}^1$ character.

C. ^{40}Ca ground state wavefunction and np-nh admixtures

The various calculations are quite different in their descriptions of the ^{40}Ca g.s. While the $0 \hbar\omega$ WBMB calculation assumes a simple closed-shell ^{40}Ca g.s. the closed-shell occupancies are 72% in the $(0+2) \hbar\omega$ WBMB calculation and 46% in the SAS calculation. In addition, the $(0+2) \hbar\omega$ WBMB calculation and SAS calculation have qualitatively different np-nh wavefunction admixtures. For example, in the SAS calculation the leading np-nh component is the $d_{3/2}^{-2}-f_{7/2}^2$ configuration with a 35% occupancy whereas in the $(0+2) \hbar\omega$ WBMB calculation the large np-nh fragmentation yields a $d_{3/2}^{-2}-f_{7/2}^2$ configuration with only 2% occupancy.

The different descriptions of the ^{40}Ca g.s. – in particular the differences in closed-shell occupancies and multi-particle, multi-hole admixtures – is the leading cause of the model-to-model variation in the calculated capture rates. It is worthwhile noting the negative-parity transitions and positive-parity transitions are endowed with qualitatively different sensitivities to the np-nh admixtures in the ^{40}Ca ground state. This difference originates as negative-parity transitions are dominantly one-body transitions connecting the ^{40}Ca closed-shell wavefunction component and the ^{40}K 1p-1h wavefunctions while the positive-parity transitions are dominantly one-body transitions connecting the ^{40}Ca 2p-2h wavefunction components and the ^{40}K 2p-2h wavefunction. Consequently, the negative-parity transitions are mostly sensitive to the magnitude of the ^{40}Ca 2p-2h admixtures while the positive-parity transitions are additionally sensitive to the configurations in the ^{40}Ca 2p-2h admixtures.

III. MUON CAPTURE CALCULATIONS

In calculating the muon capture observables and nuclear matrix elements we used the formalism and notation of Walecka [37] and Donnelly and Haxton [38] (for details see Ref. [39]). Note that in ^{40}Ca capture each $0^+ \rightarrow J_f^\pi$ transition involves a single spin-parity multipole and all observables are governed by the nuclear matrix elements of two electroweak

operators, *i.e.* $\hat{\mathcal{L}}_J - \hat{\mathcal{M}}_J$ and $\hat{\mathcal{T}}_J^{el} - \hat{\mathcal{T}}_J^{mag}$. In principle these nuclear matrix elements can involve the contributions of one-body, two-body and many-body weak nucleonic currents. Herein we assume these operators can be represented by the sum of the A one-body weak nucleonic currents, *i.e.* the impulse approximation. In such circumstances the nuclear matrix elements of $\hat{\mathcal{L}}_J - \hat{\mathcal{M}}_J$ and $\hat{\mathcal{T}}_J^{el} - \hat{\mathcal{T}}_J^{mag}$ are expressible as sums of products of single-particle matrix elements (SPMEs) and one-body transition densities (OBTDs).

In calculating the nuclear matrix elements we assumed harmonic oscillator wavefunctions with an oscillator parameter $b = 1.94$ fm. In addition, we assumed a constant muon wavefunction over the nuclear volume with $|\phi_{1s}|_{av}^2 = R|\phi_{1s}(0)|^2$ where $\phi_{1s}(0)$ is the muon wavefunction for a point-like nucleus and $R=0.44$ is the reduction factor for the ^{40}Ca nucleus [37]. In calculating the muon capture rates we generally fixed the numerically values of the weak vector, weak magnetic, weak axial and induced pseudoscalar couplings constants at $g_v = 1.0$, $g_m = 3.706$, $g_a = 1.27$ and $g_p = 8.23$. While the coupling g_p is defined at $q^2 = +0.9m_\mu^2$, the other couplings are defined at $q^2 = 0$ and therefore were scaled assuming a dipole form factor with $\Lambda^2 = 0.73$ GeV 2 . The momentum transfer q was computed via $q + q^2/2M_t = m_\mu - \Delta E - \epsilon_b$ where M_t is the target mass, m_μ is the muon mass, ϵ_b is the μ^- binding energy, and ΔE is the energy difference of the ^{40}Ca - ^{40}K nuclear states.

As mentioned above we employed harmonic oscillator wavefunctions in calculating nuclear matrix elements – such wavefunctions poorly reproducing the true asymptotic behavior of nuclear radial wavefunctions. We note the effect of different choices of radial wavefunctions in first forbidden beta-decay in $A \sim 40$ nuclei was studied by Warburton *et al.* [23]. These authors reported only small differences between the relevant nuclear matrix elements obtained with harmonic oscillator wavefunctions and Woods-Saxon wavefunctions. In particular, the $d_{3/2} \leftrightarrow p_{3/2}$ matrix elements relevant to $(0^+, 0) \rightarrow (0^-, 2626)$ capture were found to differ by roughly 5-10% (of course it is possible that their results are not applicable at the higher momentum transfer of the muon capture process). In addition, the sensitivity of weak matrix elements and muon capture rates to different radial wavefunctions was studied

in $A = 12\text{-}32$ nuclei by Kortelainen *et al* [36]. Again, in most cases these authors observed only minor differences between results derived with harmonic oscillator wavefunctions and Woods-Saxon wavefunctions.

IV. RESULTS FOR (μ^-, ν) TRANSITION RATES

In Table I we list the measured capture rates and calculated capture rates for the relevant (μ, ν) transitions to the low-lying ${}^{40}\text{K}$ states. We give the results of the WBMB and SAS calculations and the Measday and Igo-Kemenes experiments. Note that the experimental technique of γ -ray detection in Refs. [16,27] was insensitive to the ground state transition and the 30 keV state transition and that Igo-Kemenes *et al.* only quoted results for the 800, 1959 and 2047 keV states. Also note that the $0 \hbar\omega$ WBMB calculation implies a vanishing rate to the positive-parity states at 1632, 1959, 2260 and 2290 keV and the SAS calculation gives no prediction for the $d_{3/2}^{-1}p_{3/2}^1$ states at 2047, 2070, 2104 and 2626 keV.

Overall – for the ten measured rates to the low-lying ${}^{40}\text{K}$ states – we claim fair agreement between experimental data and model calculations from the perspective to the global distribution of the capture rates, *i.e.* the presence of strong, moderate and weak transitions. Clearly though – both in the comparison of experiment versus theory and model versus model – some discrepancies are obvious. We give below the detailed assessment of the capture rates for the various allowed, first-forbidden and higher-forbidden transitions. In particular, we highlight the $(0^+, 0) \rightarrow (0^-, 2626)$ axial charge transition, the $(0^+, 0) \rightarrow (2^-, 800)$ and $(0^+, 0) \rightarrow (2^-, 2047)$ unique first-forbidden transitions, and the $(0^+, 0) \rightarrow (1^+, 2290)$ allowed Gamow-Teller transition.

A. $0^+ \rightarrow 0^-$ first-forbidden transition

The capture rate for $0^+ \leftrightarrow 0^-$ transitions is determined by two nuclear matrix elements; the axial charge matrix element $M_0 \sigma \cdot \nabla$, which originates from the time component of the

axial current, and the $\ell = 1$ retarded Gamow Teller matrix element $M_{01} \cdot \sigma$, which originates from the space component of the axial current. The interest in $M_0 \sigma \cdot \nabla$ stems from its strong enhancement by pion exchange currents while the interest in $M_{01} \cdot \sigma$ term stems from the large contribution of the induced coupling g_p . Recent studies of the $^{16}\text{O}(0^+, 0) \rightarrow ^{16}\text{N}(0^-, 120)$ axial charge transition within large-basis shell model calculations have yielded values of $g_p = 6 - 9$ [40] and $g_p = 7.5 \pm 0.5$ [41] that are consistent with the theoretical prediction $g_p = 8.23$ from chiral symmetry arguments [9–11].

Our calculated rate for the $(0^+, 0) \rightarrow (0^-, 2626)$ transition as a function of the coupling g_p is shown in Fig. 2. The calculations were performed with the $0 \hbar\omega$ WBMB model and the $(0+2) \hbar\omega$ WBMB model. Fig. 2 also shows the results for (i) only the axial charge matrix element $M_0 \sigma \cdot \nabla$, (ii) only the $\ell = 1$ retarded GT matrix element $M_{01} \cdot \sigma$, and (iii) both nuclear matrix elements. Note that the curves (i), (ii) and (iii) indicate the similar magnitude and constructive interference of the two contributions (*i.e.* $M_{01} \cdot \sigma$ and $M_0 \sigma \cdot \nabla$) to the $(0^+, 0) \rightarrow (0^-, 2626)$ capture rate. Using the experimental value of $\Lambda = (15 \pm 2) \times 10^3 \text{ s}^{-1}$ for the $(0^+, 0) \rightarrow (0^-, 2626)$ rate the $0 \hbar\omega$ WBMB calculation yields a value of $g_p = 14.3^{+1.8}_{-1.6}$ and the $(0+2) \hbar\omega$ WBMB calculation yields a value of $g_p = 10.3^{+2.1}_{-1.9}$. The former value is significantly larger than, and the latter value is marginally consistent with, the theoretical prediction $g_p = 8.23$ [9–11].

Note our calculations have omitted the effects of the exchange current renormalization of the axial charge matrix element. Such effects are expected to enhance the matrix element $M_0 \sigma \cdot \nabla$ by typically a factor of two (see Ref. [42] for details). A $\sim 50\%$ enhancement of the $M_0 \sigma \cdot \nabla$ matrix element in the $(0^+, 0) \rightarrow (0^-, 2626)$ transition would further increase the calculated capture rate and thereby further increase the induced coupling g_p .

A crucial issue in the determination of the coupling g_p from the $(0^+, 0) \rightarrow (0^-, 2626)$ rate is the model uncertainties in the ^{40}Ca g.s. wavefunction. As the multi-particle, multi-hole component of the ^{40}Ca ground state is increased then the muon capture rate for the $(0^+, 0) \rightarrow (0^-, 2626)$ transition is decreased, this explaining for the lower capture rate and derived g_p -value in the $(0+2) \hbar\omega$ WBMB calculation and the higher capture rate and de-

rived g_p -value in the $0 \hbar\omega$ WBMB calculation. As discussed later in Sec. IV C, we find that neither the $0 \hbar\omega$ WBMB calculation nor the $(0+2) \hbar\omega$ WBMB calculation give a satisfactory description of the multi-particle, multi-hole admixtures in the ^{40}Ca ground state. Unfortunately, we believe this result forestalls a firm conclusion on the in-medium value of the induced pseudoscalar coupling g_p from the $(0^+, 0) \rightarrow (0^-, 2626)$ capture rate (rather we suspect that the ^{40}Ca g.s. wavefunction uncertainties are the most likely cause of the unexpectedly large value of the coupling g_p derived from the $(0^+, 0) \rightarrow (0^-, 2626)$ transition rate).

We note the effects of np-nh admixtures in first forbidden beta-decay were considered by Warburton *et al.* [23]. These authors concluded that the multi-particle multi-hole components of the nuclear wavefunctions, while yielding relatively large corrections for $\Delta J^\pi = 2^-$ first forbidden transitions, would yield relatively small corrections for $\Delta J^\pi = 0^-, 1^-$ first forbidden transitions. Specifically, they found an increase of the $M_0 \sigma \cdot \nabla$ axial charge matrix element and a decrease in the $M_{01} \cdot \sigma$ ℓ -retarded GT matrix element of roughly 10%, a small correction that would largely cancel in the $(0^+, 0) \rightarrow (0^-, 2626)$ capture rate. Herein, the apparent differences between the $0 \hbar\omega$ WBMB calculation and $(0+2) \hbar\omega$ WBMB calculation, and different closed-shell occupancies in the various model calculations, is indicative of a significantly larger model uncertainty.

B. $0^+ \rightarrow 2^-$ unique first-forbidden transitions

The experimental data also include two unique first forbidden $0^+ \rightarrow 2^-$ transitions to low-lying ^{40}K states – the $(2^-, 800)$ member of the $d_{3/2}^{-1}-f_{7/2}$ quadruplet and the $(2^-, 2047)$ member of the $d_{3/2}^{-1}-p_{3/2}$ quadruplet. The model calculations indicate both transitions are governed by the weak axial coupling g_a and the $\ell = 1$ matrix element $M_{21} \cdot \sigma$, with the $(0^+, 0) \rightarrow (2^-, 800)$ transition being dominantly $d_{3/2} \rightarrow f_{7/2}$ in character and the $(0^+, 0) \rightarrow (2^-, 2047)$ transition being dominantly $d_{3/2} \rightarrow p_{3/2}$ in character.

Concerning the $(0^+, 0) \rightarrow (2^-, 800)$ transition both model calculations and experimental data are in qualitative agreement on the very large capture rate. However, in detail the calculated rates are larger than the measured rates by factors that range from ~ 2 for the $(0+2) \hbar\omega$ WBMB model to ~ 3 for the two other models. Concerning the $(0^+, 0) \rightarrow (2^-, 2047)$ transition both model calculations and experimental data are in qualitative agreement on the rather moderate capture rate. Unfortunately the experimental results are themselves only marginally consistent, with the earlier result of Igo-Kemenes *et al.* being entirely consistent with the calculated rates while the later result of Measday and Stocki being somewhat larger than the calculated rates.

For the first forbidden $(0^+, 0) \rightarrow (2^-, 800)$ transition the analog transitions in electron scattering ${}^{40}\text{Ca}(e, e') {}^{40}\text{Ca}(8.43 \text{ MeV})$ [17–19], proton scattering ${}^{40}\text{Ca}(p, p') {}^{40}\text{Ca}(8.43 \text{ MeV})$ [43] and charge exchange ${}^{40}\text{Ca}(p, n) {}^{40}\text{Sc}(0.77 \text{ MeV})$ [20,21] are all well known. In Table II we compare the $0^+ \rightarrow 2^-$ reduced transition probability $B(M2)$ obtained from the ${}^{40}\text{Ca}(e, e')$ data [19], and the $0^+ \rightarrow 2^-$ capture rate Λ obtained from the ${}^{40}\text{Ca}(\mu, \nu)$ data [16], with the corresponding predictions of our model calculations and a pure $d_{3/2} \rightarrow f_{7/2}$ single-particle estimate. The $d_{3/2} \rightarrow f_{7/2}$ single-particle estimates are seen to exceed the measured value of $B(M2)$ by a factor 6.3 and the measured value of Λ by a factor 4.6. By comparison the model calculations are seen to exceed the measured values of $B(M2)$ by factors of 1.5-3.1 and the measured values of Λ by factors of 1.6-2.8. The similar quenching for the $0^+ \rightarrow 2^-$ transition in the muon capture data and the electron scattering data is not surprising, both processes being dominated by the matrix element of the spin-dipole ($M_{21} \cdot \sigma$) operator. Comparable quenching is also reported for the analog transitions in the ${}^{40}\text{Ca}(p, p')$ data and the ${}^{40}\text{Ca}(p, n)$ data.

This quenching or hindrance of the measured rate over the calculated rate – as observed for the (μ^-, ν) capture rate and the (e, e') reduced transition probability to the $(2^-, 800)$ state – is well documented for unique first-forbidden β -decay in mass $A \sim 40$ nuclei (for example see Warburton *et al.* [23]). As documented in detail by Towner *et al.* [44], such quenching originates from the repulsive character of the $T = 1$ particle-hole interaction and

its coherent effects on the particle-hole admixtures in the initial-final state wavefunctions. In particular, in Ref. [23] the authors report a typical hindrance of approximately 3.7 for the known unique first-forbidden β -decay transitions in the $A \sim 40$ mass region in a global comparison to their WBMB calculations.

By comparison we observe no hindrance of the measured capture rate compared to the calculated capture rate for the $(0^+, 0) \rightarrow (2^-, 2047)$ transition. Interesting, the $(0^+, 0) \rightarrow (2^-, 2047)$ transition is dominantly $d_{3/2} \rightarrow p_{3/2}$ in character whereas the $(0^+, 0) \rightarrow (2^-, 800)$ transition is dominantly $d_{3/2} \rightarrow f_{7/2}$ character (the unique first-forbidden beta decays in the $A \sim 40$ mass region are also $d_{3/2} \rightarrow f_{7/2}$ transitions). As described by Towner *et al.* [44], the hindrances associated with $T = 1$ particle-hole interactions are dependent on the orbital angular momenta of the particular transition, and might differ between the $d \rightarrow f$ angular momenta of the $(0^+, 0) \rightarrow (2^-, 800)$ transition and the $d \rightarrow p$ angular momenta of the $(0^+, 0) \rightarrow (2^-, 2047)$ transition (of course it would be premature to draw any such conclusion from a data-set of two $0^+ \rightarrow 2^-$ transitions).

C. $0^+ \rightarrow 1^+$ allowed Gamow-Teller transition

The leading contribution to $0^+ \rightarrow 1^+$ transitions originates from the weak axial coupling constant g_a and the spin-flip matrix element $M_{10} \cdot \sigma$. Since the $M_{10} \cdot \sigma$ matrix element vanishes in a simple closed-shell description of the ${}^{40}\text{Ca}$ ground state such $0^+ \rightarrow 1^+$ transitions are especially sensitive to the np-nh admixtures in the ${}^{40}\text{Ca}$ g.s. wavefunction.

As discussed in Sec. II C the specific np-nh admixtures in the ${}^{40}\text{Ca}$ g.s. are strikingly different in the SAS model, 0 $\hbar\omega$ WBMB model, and (0+2) $\hbar\omega$ WBMB model. In the SAS calculation the $(0^+, 0) \rightarrow (1^+, 2290)$ transition is dominated by a large $d_{3/2} \rightarrow d_{3/2}$ one-body transition density that originates from the large $d_{3/2}^{-2} \cdot f_{7/2}^{-2}$ admixture in the ${}^{40}\text{Ca}$ g.s. wavefunction. In the (0+2) $\hbar\omega$ WBMB calculation the $(0^+, 0) \rightarrow (1^+, 2290)$ transition is comprised of many small one-body transition densities that originate from the fragmented

np-nh admixtures in the ^{40}Ca g.s. wavefunction. Consequently, the calculated $(0^+, 0) \rightarrow (1^+, 2290)$ rate is relatively large in the SAS model ($19.2 \times 10^3 \text{ s}^{-1}$) and relatively small in the $(0+2) \hbar\omega$ WBMB model ($0.08 \times 10^3 \text{ s}^{-1}$). The measured rate $(13 \pm 5) \times 10^3 \text{ s}^{-1}$ is slightly smaller than the SAS prediction but much larger than the $(0+2) \hbar\omega$ WBMB prediction, thus suggesting a better treatment of the np-nh admixtures in the ^{40}Ca g.s. wavefunction by the SAS model.

This conclusion is supported by the inelastic electron scattering data for the $^{40}\text{Ca}(e, e')^{40}\text{Ca}(1^+, 9.87 \text{ MeV})$ analog transition. This transition was studied by Petraitis *et al.* [19] and yielded a reduced transition probability of $B(\text{M1}) = 0.32 \pm 0.09 \mu_N^2$ to be compared with a SAS prediction of $B(\text{M1}) = 0.86 \mu_N^2$ and a $(0+2) \hbar\omega$ WBMB prediction of $B(\text{M1}) \simeq 0.01 \mu_N^2$. The moderate over-prediction of $B(\text{M1})$ by the SAS model and gross under-prediction of $B(\text{M1})$ by the WBMB model is quite similar to the corresponding comparisons between the calculated rates and the measured rates in the μ capture reaction. The similar scaling between experimental values and model values in μ capture and (e, e') scattering is not surprising as both processes are dominated by the spin-flip $M_{10} \cdot \sigma$ matrix element.

As a final demonstration of the high sensitivity of the $(0^+, 0) \rightarrow (1^+, 0)$ transition to the np-nh components in the $A = 40$ wavefunctions we list in Table III the $(0^+, 0) \rightarrow (1^+, 2290)$ capture rate versus the maximum occupancy of the $f_{7/2}$ orbital in the SAS model. It clearly shows the strong correlation between the $0^+ \rightarrow 1^+$ transition rate and the np-nh admixtures in the ^{40}Ca , 0^+ ground state and the ^{40}K , 1^+ excited state. For example, by increasing the SAS model space from 0-2 $\hbar\omega$ to 0-8 $\hbar\omega$ one increases the $0^+ \rightarrow 1^+$ capture rate from $4.7 \times 10^3 \text{ s}^{-1}$ to $19.2 \times 10^3 \text{ s}^{-1}$.

D. Other transition

The remaining transitions comprise the $(0^+, 0) \rightarrow (0^+, 1632)$ non-analog Fermi transition,

the $(0^+, 0) \rightarrow (1^-, 2104)$ mixed first-forbidden transition, and four $\ell > 1$ forbidden transitions that range from second-forbidden to fifth-forbidden.

The leading contribution to $(0^+, 0) \rightarrow (0^+, 1632)$ transition originates from the weak vector coupling constant g_v and the nuclear matrix element M_0 . As discussed earlier the transition rates for low-lying positive-parity states are highly sensitive to the multi-particle, multi-hole admixtures in the ${}^{40}\text{Ca}$ ground state. In the SAS calculation the transition involves the destructive interference of $d_{3/2} \rightarrow d_{3/2}$ and $f_{7/2} \rightarrow f_{7/2}$ s.p. transitions and yields a capture rate $1.2 \times 10^3 \text{ s}^{-1}$. In the $(0+2)$ $\hbar\omega$ WBMB model the transition involves many small contributions from different s.p. transitions that destructively interfere and yield a capture rate $0.01 \times 10^3 \text{ s}^{-1}$. Like the $(0^+, 0) \rightarrow (1^+, 2290)$ transition the large differences in calculated rates are a consequence of the differences in the multi-particle, multi-hole admixtures in the ${}^{40}\text{Ca}$ g.s. model wavefunctions. The measured rate of $(13 \pm 10) \times 10^3 \text{ s}^{-1}$ has large uncertainties and is consistent with both calculations.

The leading contribution to $(0^+, 0) \rightarrow (1^-, 2104)$ transition originates from the weak axial coupling constant g_a and the nuclear matrix element $M_{11} \cdot \sigma$. The transition to this $d_{3/2}^{-1} p_{3/2}^1$ particle-hole state is dominated by the $d_{3/2} \rightarrow p_{3/2}$ single particle transition. The measured rate of $(18 \pm 5) \times 10^3 \text{ s}^{-1}$, $0 \hbar\omega$ WBMB rate of $14.7 \times 10^3 \text{ s}^{-1}$, and $(0+2)$ $\hbar\omega$ WBMB rate of $9.0 \times 10^3 \text{ s}^{-1}$, are consistent within 1-2 standard deviations.

The various model calculations for the four $\ell > 1$ forbidden transitions all imply small capture rates. While the measured rate for the fifth-forbidden $0^+ \rightarrow (5^-, 891)$ transition and the third-forbidden $0^+ \rightarrow (3^+, 2260)$ transition are reasonably consistent with model predictions, the third forbidden $0^+ \rightarrow (3^-, 2070)$ transition and second forbidden $0^+ \rightarrow (2^+, 1959)$ transition have unexpectedly large measured rates for $\ell = 2, 3$ forbidden transitions. We speculate – as mentioned by Measday and Stocki [16] – that their experimental capture rates may include unidentified cascade feeding from higher-lying ${}^{40}\text{K}$ levels.

V. RECOIL LONGITUDINAL ALIGNMENT

Both $0^+ \rightarrow 1^+$ and $0^+ \rightarrow 2^-$ transitions involve contributions from the induced pseudoscalar coupling constant g_p . While the contribution of g_p to their capture rates is generally quite small the contribution of g_p to their longitudinal alignments are frequently rather large.² Given the observation of $0^+ \rightarrow 1^+$ and $0^+ \rightarrow 2^-$ transitions in $^{40}\text{Ca}(\mu, \nu)$ capture, and determinations of the analogous transition probabilities in $^{40}\text{Ca}(e, e')$ scattering, we thought it interesting to consider the possibility of determining g_p by measuring the ^{40}K alignment following ^{40}Ca capture. Such measurements were previously performed for muon capture on ^{14}N [45], ^{28}Si [46] and ^{35}Cl [47].

Figs. 3 and 4 give results for the longitudinal alignment a_2 versus the induced coupling g_p for the $0^+ \rightarrow (2^-, 800)$ transition and the $0^+ \rightarrow (1^+, 2290)$ transition using the SAS model (we adopt the SAS model rather than the WBMB model as it reasonably reproduces both the capture rates). Shown are results using (i) all the contributing nuclear matrix elements and (ii) only the leading matrix elements (either $M_{10} \cdot \sigma$ or $M_{21} \cdot \sigma$). In addition, we plot the results with maximum $f_{7/2}$ occupancies of either four nucleons or eight nucleons in order to gauge the model dependences. Concerning the $0^+ \rightarrow 2^-$ transition the calculation shows a relatively low sensitivity to both the coupling g_p and the nuclear wavefunctions, the wavefunction insensitivity reflecting the dominance of the $f_{7/2}^1 d_{3/2}^{-1}$ transition and the $M_{21} \cdot \sigma$ matrix element. Concerning the $0^+ \rightarrow 1^+$ transition the calculation shows both greater sensitivity to the coupling g_p and greater sensitivity to the nuclear wavefunctions, the wavefunction sensitivity reflecting the interference between $d_{3/2} \rightarrow d_{3/2}$ and $f_{7/2} \rightarrow f_{7/2}$

²The recoil orientation about the neutrino momentum is termed the longitudinal orientation and the recoil orientation about the muon spin is termed the average orientation. For $J \geq 1$ recoils the orientation includes both a recoil polarization (rank-one orientation) and a recoil alignment (rank-two orientation). We consider the longitudinal alignment a_2 which is experimentally accessible in the γ -ray experiments.

single-particle transitions and $M_{10} \cdot \sigma$ and $M_1 \sigma \cdot \nabla$ matrix elements.

Could the longitudinal alignments in $0^+ \rightarrow (2^-, 800)$ transitions or $0^+ \rightarrow (1^+, 2290)$ transitions be measured? In certain cases the alignment imparts a directional correlation between the recoil nucleus and the subsequent de-excitation γ -ray [49], and is thereby measurable by the γ -ray Doppler lineshape. However, such measurements require both a suitable γ -decay spin sequence and a short γ -decay lifetime. Specifically, the γ -recoil directional correlation $W(\theta)$ is given by

$$W(\theta) \propto 1 + a_2 B_{21} P_2(\cos \theta) \quad (1)$$

where $P_2(\cos \theta)$ is the Legendre polynomial, θ the angle between the recoil direction and the γ -ray direction, and B_{21} the γ -radiation coefficient (see Ref. [48] for details). For the $0^+ \rightarrow 1^+$ transition the dominant M1 decay $(1^+, 2290) \rightarrow (0^+, 1644)$ [50] yields $B_{21} = 1/\sqrt{2}$ which implies a comparatively high sensitivity to a_2 . For the $0^+ \rightarrow 2^-$ transition the dominant M1 decay $(2^-, 800) \rightarrow (3^-, 30)$ [50] yields $B_{21} = 1/\sqrt{70}$ which implies a comparatively low sensitivity to a_2 . In addition, the lifetime for the gamma de-excitation must either be shorter or comparable to the slowing-down time of the recoil ion. Here the $0^+ \rightarrow 1^+$ lifetime of 83 fs and the $0^+ \rightarrow 2^-$ lifetime of 280 fs are comparable to the recoil slowing-down time of ~ 250 fs [51]. In short, we suspect such measurements are possible but challenging.

VI. SUMMARY

In summary we report the calculation of partial rates and recoil orientations in muon capture on calcium-40. The calculations were performed with well-established, well-tested nuclear models: the WBMB interaction and sd-pf model space of Warburton *et al.* [30] and the SAS interaction and $d_{3/2}$ - $f_{7/2}$ model space of Sakakura *et al.* [34]. Moreover, the WBMB calculations were performed with both a simple closed-shell ${}^{40}\text{Ca}$ ground state and a mixed $(0+2)$ $\hbar\omega$ ${}^{40}\text{Ca}$ ground state. Taken together the calculations were capable of reproducing the important features of low-lying negative and positive parity ${}^{40}\text{K}$ levels.

Overall we observed fair agreement between measured capture rates and calculated cap-

ture rates for the low-lying ^{40}K levels, *i.e.* the general distribution of muon capture rates to low-lying ^{40}K levels being reasonably consistent between the model calculations and the experimental results. We note however two striking exceptions – the third forbidden $0^+ \rightarrow (3^-, 2070)$ transition and second forbidden $0^+ \rightarrow (2^+, 1959)$ transition – for which the measured rates exceeded the calculated rates by very large factors.

Most importantly we emphasized the $(0^+, 0) \rightarrow (0^-, 2626)$ axial charge transition and its high sensitivity to the induced pseudoscalar coupling g_p of the proton's weak interaction. Using the measured capture rate of Measday and Stocki [16] our $(0+2) \hbar\omega$ WBMB calculation yielded $g_p = 10.3_{-1.9}^{+2.1}$ and our $0 \hbar\omega$ WBMB calculation yielded $g_p = 14.3_{-1.6}^{+1.8}$. Unfortunately, we concluded that neither the simpler $0 \hbar\omega$ WBMB calculation nor the richer $(0+2) \hbar\omega$ WBMB calculation were capable of satisfactorily describing the multi-particle, multi-hole admixtures in the ^{40}Ca ground state, thus forestalling a firm conclusion on the in-medium value of the coupling constant g_p from the $(0^+, 0) \rightarrow (0^-, 2626)$ transition rate.

The above deficiencies in the model descriptions of the ^{40}Ca ground state were highlighted by our discussion of the $(0^+, 0) \rightarrow (1^+, 2290)$ allowed Gamow-Teller transition. Such $0^+ \rightarrow 1^+$ transitions on doubly-magic ^{40}Ca are especially sensitive to the np-nh admixtures in the ^{40}Ca ground state as the $M_{10} \cdot \sigma$ spin-flip matrix element vanishes for a simple closed-shell wavefunction. Unfortunately, we found large model-to-model variations in the different calculations of the $(0^+, 0) \rightarrow (1^+, 2290)$ capture rate, and most worrisome for the analysis of the $(0^+, 0) \rightarrow (0^-, 2626)$ transition, the $(0+2) \hbar\omega$ WBMB calculation grossly under-estimates the $(0^+, 0) \rightarrow (1^+, 2290)$ transition rate.

In addition, we discussed two $0^+ \rightarrow 2^-$ unique first forbidden transitions to ^{40}K levels at 800 and 2047 keV. In nuclear beta-decay such first-forbidden transitions have been extensively studied in the context of their hindrance via the coherent effects of the repulsive $T=1$ particle-hole interaction. Intriguingly, we found a substantial hindrance of the $(0^+, 0) \rightarrow (2^-, 800)$ transition that has dominant $d_{3/2} \rightarrow f_{7/2}$ character but a negligible hindrance of the $(0^+, 0) \rightarrow (2^-, 2047)$ transition that has dominant $d_{3/2} \rightarrow p_{3/2}$ character. The latter case of a $d_{3/2} \rightarrow p_{3/2}$ transition is generally inaccessible via the β -decay studies in the

$A \sim 40$ mass region.

A number of improvements could be made on our work. The calculations were conducted using limited model spaces, harmonic oscillator nuclear wavefunctions, and uniform muonic wavefunctions. In particular, the multi-particle, multi-hole structure of ^{40}Ca ground state was a major difficulty for the model calculations, it limiting our conclusions for the induced coupling g_p in the $(0^+, 0) \rightarrow (0^-, 2626)$ transition. Given the sensitivity of the $0^+ \rightarrow 0^-$ axial charge transition to the induced pseudoscalar coupling, the interest in the $0^+ \rightarrow 2^-$ unique first forbidden transitions due to core polarization effects, and the interest in the $0^+ \rightarrow 1^+$ allowed Gamow-Teller transitions due to ground state correlations, we strongly encourage further theoretical work on ^{40}Ca muon capture. In addition, new experimental efforts on exclusive muon capture in other $A \sim 40$ nuclei would help to extend the experimental data-set and benefit any model studies.

We wish to thank both Prof. David Measday and Dr. Trevor Stocki for valuable discussions and gratefully acknowledge the National Science Foundation (USA) for their financial support.

TABLES

TABLE I. Comparison of measured rates and calculated rates for muon capture to low-lying ^{40}K levels. The first two columns list the spin-parities and excitation energies of the ^{40}K states and the final column lists the dominant particle-hole configurations of the ^{40}K states. The experimental rates are taken from the experimental work of Measday and Stocki (column three) and Igo-Kemenes *et al* (column four) and the calculated rates were obtained with the SAS, 0 $\hbar\omega$ WBMB, and (0+2) $\hbar\omega$ WBMB models (see text for details).

J_f^π	E_x (keV)	Exp. [16] (10^3 s $^{-1}$)	Exp. [27] (10^3 s $^{-1}$)	SAS rate (10^3 s $^{-1}$)	0 $\hbar\omega$ WBMB (10^3 s $^{-1}$)	(0+2) $\hbar\omega$ WBMB (10^3 s $^{-1}$)	dominant p-h config.
4 $^-$	0			3.2	2.7	1.7	$(d_{3/2})^{-1}(f_{7/2})^1$
3 $^-$	30			7.0	3.4	2.1	$(d_{3/2})^{-1}(f_{7/2})^1$
2 $^-$	800	127 \pm 13	108 \pm 30	339	351	200	$(d_{3/2})^{-1}(f_{7/2})^1$
5 $^-$	891	5.1 \pm 2.5		0.0	0.0	0.0	$(d_{3/2})^{-1}(f_{7/2})^1$
0 $^+$	1632	13 \pm 10		1.2	0.0	0.0	$(d_{3/2})^{-2}(f_{7/2})^2$
2 $^+$	1959	31 \pm 5	13 \pm 5	5.8	0.0	0.2	$(d_{3/2})^{-2}(f_{7/2})^2$
2 $^-$	2047	21 \pm 7	12 \pm 4		11.5	7.4	$(d_{3/2})^{-1}(p_{3/2})^1$
3 $^-$	2070	18 \pm 7			0.8	0.6	$(d_{3/2})^{-1}(p_{3/2})^1$
1 $^-$	2104	18 \pm 5			14.7	9.0	$(d_{3/2})^{-1}(p_{3/2})^1$
3 $^+$	2260	<6		0.0	0.0	0.0	$(d_{3/2})^{-2}(f_{7/2})^2$
1 $^+$	2290	13 \pm 5		19.2	0.0	0.08	$(d_{3/2})^{-2}(f_{7/2})^2$
0 $^-$	2626	15 \pm 2			23.2	17.2	$(d_{3/2})^{-1}(p_{3/2})^1$

TABLE II. Comparison of measured and calculated muon capture rates Λ , and measured and calculated reduced transition probabilities $B(M2)$, for the $(0^+,0) \rightarrow (2^-, 800)$ unique first forbidden transition. Column three lists the $d_{3/2} \rightarrow f_{7/2}$ single-particle estimate and columns four, five and six list the results of the SAS, 0 $\hbar\omega$ WBMB and (0+2) $\hbar\omega$ WBMB models (see text for details).

observable	measured	$d_{3/2} \rightarrow f_{7/2}$	SAS	0 $\hbar\omega$ WBMB	(0+2) $\hbar\omega$ WBMB
	value	s.p. estimate	model	model	model
$B(M2)$ (μ_N^2 fm 2)	235±20	1495	778	692	375
Λ ($\times 10^3$ s $^{-1}$)	127±13	600	339	351	200

TABLE III. The calculated muon capture rate for the $(0^+,0) \rightarrow (1^+, 2290 \text{ keV})$ allowed Gamow-Teller transition versus the maximum occupancy of the $f_{7/2}$ occupancy. Also given are the 2p-2h and 4p-4h admixtures in the ^{40}Ca and ^{40}K wavefunctions.

maximum $f_{7/2}$ occupancy	^{40}Ca 2p-2h admixture (%)	^{40}Ca 4p-4h (%)	^{40}K 2p-2h admixture (%)	^{40}K 4p-4h admixture (%)	rate ($\times 10^3 \text{ s}^{-1}$)
2	27.0		100		4.7
4	35.7	8.9	71.3	28.7	11.0
6	35.5	13.6	56.5	36.0	16.8
8	35.0	14.5	52.5	36.3	19.2

FIGURES

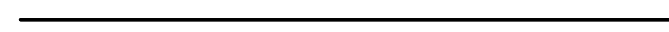
$(d_{3/2})^{-2} (f_{7/2})^2$	2.289		1^+
$(d_{3/2})^{-2} (f_{7/2})^2$	2.26		3^+
$(d_{3/2})^{-1} (p_{3/2})^1$	2.103		1^-
$(d_{3/2})^{-1} (p_{3/2})^1$	2.069		3^-
$(d_{3/2})^{-1} (p_{3/2})^1$	2.047		2^-
$(d_{3/2})^{-2} (f_{7/2})^2$	1.959		2^+
$(d_{3/2})^{-2} (f_{7/2})^2$	1.643		0^+
$(d_{3/2})^{-1} (f_{7/2})^1$	0.891		5^-
$(d_{3/2})^{-1} (f_{7/2})^1$	0.8		2^-
$(d_{3/2})^{-1} (f_{7/2})^1$	0.029		3^-
$(d_{3/2})^{-1} (f_{7/2})^1$	0		4^-

FIG. 1. Summary of assignments of model states to experimental states for the low-lying ^{40}K levels. Shown are the spin-parities, excitation energies, and dominant particle-hole configurations for the low-lying ^{40}K states.

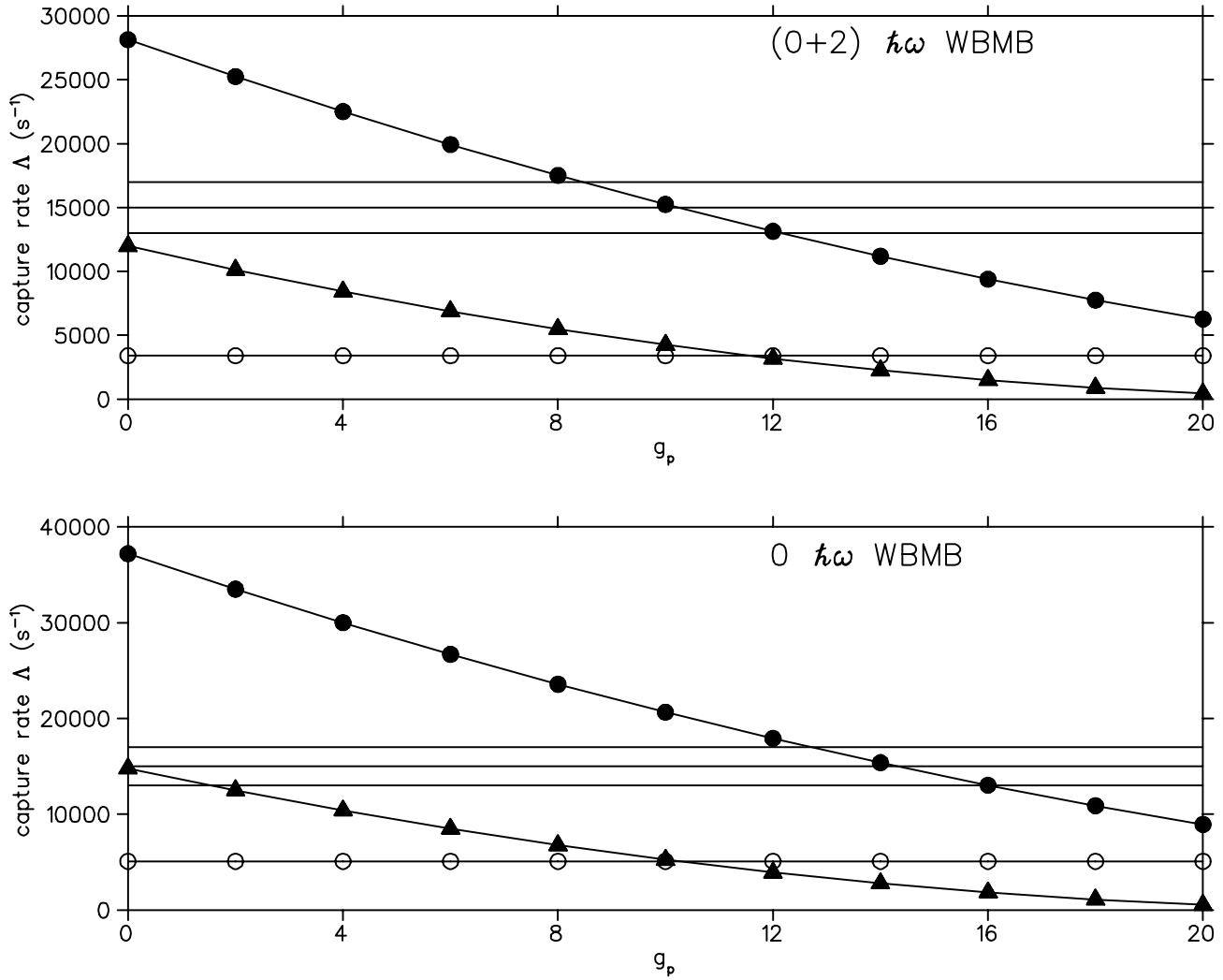


FIG. 2. Calculated rate for the $(0^+, 0) \rightarrow (0^-, 2626)$ transition as a function of the coupling constant g_p from the $(0+2) \hbar\omega$ WBMB calculation (upper panel) and the $0 \hbar\omega$ WBMB calculation (lower panel). The open circles correspond to the axial charge matrix element only, the filled triangles correspond to the $\ell = 1$ retarded GT matrix element only, and the filled circles correspond to the full calculation. The measured rate $\Lambda = (15 \pm 2) \times 10^3 \text{ s}^{-1}$ is shown by the horizontal lines.

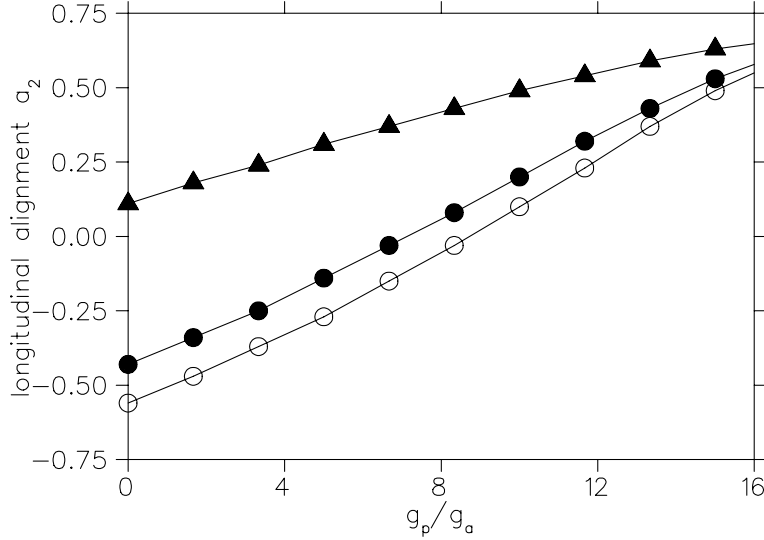


FIG. 3. Calculation of the longitudinal alignment a_2 for the $0^+ \rightarrow (1^+, 2290)$ transition versus the coupling g_p . The solid circles indicate the SAS calculation permitting up to eight particles in the $f_{7/2}$ orbital and the open circles indicate the SAS calculation permitting up to four particles in the $f_{7/2}$ orbital. The calculation employing only the $M_{10} \cdot \sigma$ matrix element is denoted by triangles.

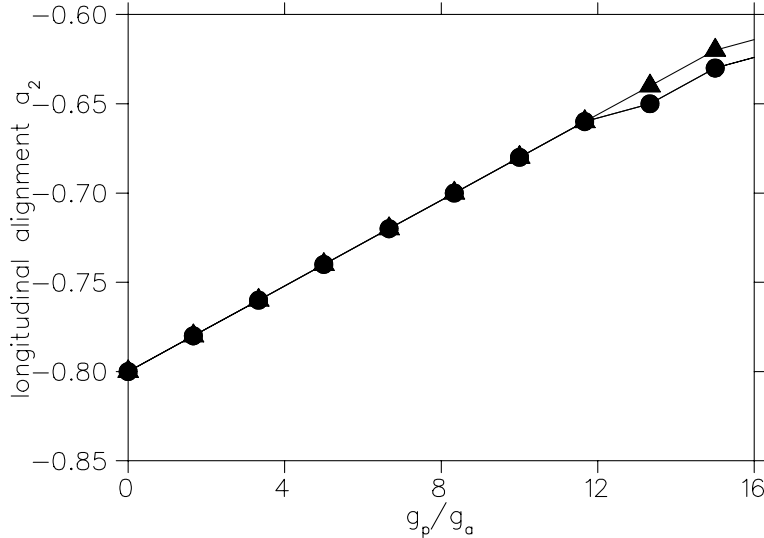


FIG. 4. Calculation of the longitudinal alignment a_2 for the $0^+ \rightarrow (2^-, 800)$ transition versus the coupling g_p . The solid circles indicate the SAS calculation permitting up to eight particles in the $f_{7/2}$ orbital and the open circles indicate the SAS calculation permitting up to four particles in the $f_{7/2}$ orbital. The calculation employing only the $M_{21} \cdot \sigma$ matrix element is denoted by triangles.

REFERENCES

- [1] E.J. Maier, B.L. Bloch, R.M. Edelstein, and R.T. Siegel, Phys. Rev. Lett. **6**, 417, (1961).
- [2] G. Culligan, J.F. Lathrop, V.L. Telegdi, R. Winston, and R.A. Lundy, Phys. Rev. Lett. **7**, 458 (1961).
- [3] Valentine L. Telegdi, Phys. Rev. Lett. **8**, 327, (1962).
- [4] T. Gorringe and H. W. Fearing, Rev. Mod. Phys. **76**, 31 (2004).
- [5] B. R. Holstein, Phys. Rev. D **13**, 2499 (1976).
- [6] C. Leroy and L. Palfy, Phys. Rev. D **15**, 924 (1977).
- [7] Y. Shitov *et al.*, Nucl. Phys. A **699**, 917 (2002).
- [8] D.F. Measday, Phys. Rept. **354**, 243 (2001).
- [9] M. L. Goldberger and S. B. Treiman, Phys. Rev. **111**, 354 (1958).
- [10] V. Bernard, N. Kaiser and Ulf-G. Meissner, Phys. Rev. D **50**, 6899 (1994).
- [11] Harold W. Fearing, Randy Lewis, Nader Mobed, and Stefan Scherer, Phys. Rev. D **56**, 1783 (1997).
- [12] J. Delorme, M. Ericson, A. Figureau, and C. Thévenet, Ann. Phys. (NY) **102**, 273 (1976).
- [13] J. Delorme and M. Ericson, Phys. Rev. C **49**, R1763 (1994).
- [14] M. Rho, Ann. Rev. Nucl. and Part. Science **34**, 531 (1984).
- [15] M. Gmitro and P. Truoel, Adv. Nucl. Phys. **18**, 241 (1987).
- [16] D.F. Measday and T.J. Stocki, Phys. Rev. C **73**, 045501 (2006).
- [17] P.E. Burt, L.W. Fagg, H.Crannell, D.I. Sober, W. Stapor, J.T. O'Brien, X.K. Maruyama, J.W. Lightbody, and R.A. Lindgren, Phys. Rev. C —bf 25, 2805

(1982).

- [18] S. Oguro, Y. Mizuno, T. Terasawa, Y. Torizuka, Y. Kawazoe and K. Arita, Phys. Rev. C **30**, 1159 (1984).
- [19] M. Petraitis, J.P. Connelly, H. Crannell, L.W. Fagg, J.T. O'Brien, D.I. Sober, J.R. Deininger, S. E. Williamson and S. Raman, Phys. Rev. C **51**, 1014 (1995).
- [20] T. N. Taddeucci *et al.*, Phys. Rev. C **28**, 2511 (1983).
- [21] T. Chitrakarn, B.D. Anderson, A.R. Baldwin, C. Lebo, R. Madey, J.W. Watson and C.C. Foster, Phys. Rev. C **34**, 80 (1986).
- [22] E.K. Warburton, D.E. Alburger, J.A. Becker, B.A. Brown and S. Raman, Phys. Rev. C**34**, 1031 (1986).
- [23] E.K. Warburton, J.A. Becker, B.A. Brown and D.J. Millener, Ann. Phys. **187**, 471 (1988).
- [24] E.K. Warburton and J.A. Becker, Phys. Rev. C **37**, 754 (1988).
- [25] E.K. Warburton and D.E. Alburger Phys. Rev. C **38**, 2822 (1988).
- [26] E.K. Warburton, J.A. Becker, B.A. Brown, Phys. Rev. C **41**, 1147 (1990).
- [27] P. Igo-Kemenes, J.P. Deutsch, D. Favart, L. Grenacs, P. Lipnik and P.C. Macq, Phys. Lett. **34B**, 286 (1971).
- [28] C.K. Davis, G.D. Jones, I.G. Main, B.T. McCrone, M.F. Thomas and P.J. Twin, J. Phys. **A6**, 844 (1973).
- [29] B.A. Brown, A. Etchegoyen, W. D. M. Rae, and N. S. Godwin, MSUCL Report No. 524 (1986).
- [30] E.K. Warburton and J.A. Becker, Phys. Rev. C **40**, 2823 (1989).
- [31] B.H. Wildenthal, Prog. Part. Nucl. Phys. **11**, 5 (1984).

- [32] J.B. McGrory, Phys. Rev. C **8**, 693 (1973).
- [33] D.J. Millener and D. Kurath, Nucl. Phys. **A255**, 315 (1975).
- [34] M. Sakakura, A. Arima and J. Sebe, Phys. Lett. **61B**, 335 (1976).
- [35] P.M. Endt, At. Data Nucl. Data Tables **19**, 23 (1977).
- [36] M. Kortelainen, M. Aunola, T. Siiskonen and J. Suhonen, J. Phys. G Nucl. Part. Phys. **26**, L33 (2000).
- [37] J.D. Walecka, in Muon Physics, C.S. Wu and V. Hughes eds., Academic Press, NY, (1975).
- [38] T.W. Donnelly and W.C. Haxton, At. Data Nucl. Data Tables **23**, 103 (1979).
- [39] B.L. Johnson, T. P. Gorrige, D. S. Armstrong, J. Bauer, M. D. Hasinoff, M. A. Kovash, D. F. Measday, B. A. Moftah, R. Porter, and D. H. Wright, Phys. Rev. C **54**, 2714 (1996).
- [40] W. Haxton and C. Johnson, Phys. Rev. Lett. **65**, 1325 (1990).
- [41] E.K. Warburton, I.S. Towner and B.A. Brown Phys. Rev. C **49**, 824 (1994).
- [42] I S Towner, Ann. Rev. of Nucl. Part. Science. **36**, 115 (1986)
- [43] H. Ejiri, M. Sasao, T. Shibata, H. Ohsumi, Y. Fujita, M. Fujiwara, T. Yamazaki, I. Katayama, S. Morinobu, and H. Ikegami, Phys. Rev. C **24**, 2001 (1981).
- [44] I.S. Towner, E.K. Warburton and G.T. Garvey, Ann. Phys. **66**, 674 (1971).
- [45] T.P. Gorrige, D.P. Corbin and T.J. Stocki, Phys. Rev. C **71**, 035503 (2005).
- [46] B.A. Moftah *et al.*, Phys. Lett. B **395**, 157 (1997).
- [47] S. Arole *et al.*, Phys. Rev. C **66**, 065501 (2002).
- [48] S. Ciechanowicz and Z. Oziewicz, Fortsch. Phys. **32**, 61 (1984).

[49] L. Grenacs, J.P. Deutsch, P. Lipnik, and P.C. Macq, Nucl. Instrum. Methods **58**, 164 (1968).

[50] Evaluated Nuclear Structure Data File (8/1/2004). National Nuclear Data Center, Brookhaven National Laboratory.

[51] SRIM program, J.F.Ziegler. See J.P. Biersack, J.F. Ziegler and U. Littmark, *The stopping and range of ions in solids*, Pergamon Press (1985).